This is a peer-reviewed, author's accepted manuscript of the following research article:
Wu, H., Liu, H., Xue, Z., Yang, J., Li, Q., He, D., & Siew, W. H. (2022). The generation and migration of bubbles in oil-pressboard insulation needle-plate system. IEEE Transactions on Dielectrics and Electrical Insulation . https://doi.org/10.1109/tdei.2022.3210486

The Generation and Migration of Bubbles in Oil-Pressboard Insulation Needle-Plate System

Hongbin Wu, Hongshun Liu*, Member, IEEE, Zhitong Xue, Jingjing Yang,

Qingquan Li, Dongxin He, Wah Hoon Siew

***Abstract*—Bubbles in transformer oil can easily lead to partial discharge, which can deteriorate the transformer oil and even breakdown the transformer insulation. To clarify the migration process and the characteristics of bubbles generated in an oil-immersed power transformer exposed to an extremely uneven electric field, we experimentally monitor these phenomena under an extremely nonuniform AC electric field and numerically simulate the migration distance and the migration speed of bubbles with different initial positions and sizes. The results show that the streamer discharge channel formed by a partial discharge in oil is gasified into a bubble channel. After it collides with the surface of the pressboard, its morphology is transformed into approximately spherical bubbles due to the surface tension of the gas-liquid interface. After bubbles are generated in the oil, they move away from areas with a strong electric field due to the electric-field force and gradually approach the oil surface due to the buoyancy force. The experimental results are consistent with the simulation results, which verify the rationality of the simulation model.**

***Index Terms*—bubbles, migration process and characteristic, partial discharge, oil-immersed power transformer**

I. Introduction

As the core equipment of power system, the reliable operation of the power transformer is closely related to the safety and stability of the entire system [1–4]. Unfortunately, transformer-insulation failure has been an all-too-common occurrence in recent years [5–8]. During the long-term operation of transformers, they inevitably experience partial overheating, partial discharge (PD), and vibration (or they are simply subject to human error), which forms bubbles in the transformer oil [9–11]. Bubbles in insulating oil may cause PD where the insulation is weak. The thermal effect and corona caused by PD and acoustic cavitation caused by voltage shocks also produce bubbles in the insulating oil [12]. Given an increasing number of bubbles in the oil, they may easily aggregate to form bubble bridges, which further deteriorate the transformer oil and can even cause insulation failure in the transformer [13–15]. The dynamic behavior of bubbles will cause gap discharge of insulating oil, and even lead to oil gap breakdown, which will lead to the failure of the transformer insulation. Therefore, studying the dynamic characteristics of bubbles is of great significance for preventing transformer insulation damage, and also has important engineering application value in actively enhancing heat transfer, and the migration characteristics of bubbles are the key to explaining the dynamic behavior of bubbles.

Research into the migration and accumulation characteristics of bubbles under composite AC-DC electric fields shows that bubbles move along electric-field lines and converge on equipotential surfaces [16]. Photographing the bubble positions over time in a horizontal oil pipeline allows one to analyze how temperature and applied voltage affect the trajectory of bubbles in horizontal oil pipelines. The results show that the movement of bubbles is divided into two phases: a rising phase and a horizontal phase [17,18]. However, these studies assume a uniform electric field when discussing bubble migration. In a power transformer, the electric field is complex, with an intense electric field in the oil gap and an extremely uneven electric-field distribution. Therefore, it is important to use an oil-pressboard insulation needle-plate system to simulate an oil-immersed power transformer exposed to an extremely uneven electric field. By using numerical simulations to study the dynamic characteristics of bubbles in oil under an AC electric field. The results show that an oscillation equilibrium position appears in areas of intense electric field [19]. Numerous previous experiments have studied how oil flow velocity affects bubble motion and the bubble-breakdown characteristics of insulating oil [20,21]. These experiments monitored the movement and migration process of bubbles in oil under uneven AC electric fields, and the migration path and rate of bubble formation were analyzed as a function of electric field intensity by numerical simulation. The results indicate that the Coulomb force accelerates the upward movement of bubbles [12]. Note that these studies were all based on the artificially produced bubbles, whereby bubbles of regular shape and uniform size were produced in the insulating oil by using a gas pump, and then their dynamic characteristics were observed. Thus, such studies do not reproduce the randomness in location, size, shape, and number of bubbles that occurs in the real

This work has been supported by the Natural Science Foundation of Shandong Province (No. ZR2020ME196) and the National Natural Science Foundation of China (No. U1966209) .

Hongbin Wu, Hongshun Liu, Jingjing Yang, Qingquan Li, Dongxin He are with Shandong Provincial Key Laboratory of UHV Transmission Technology and Equipment School of Electrical Engineering, Shandong University, Jinan, China. (e-mail: 734977611@qq.com, lhs@sdu.edu.cn, 22808156@qq.com, lqq@sdu.edu.cn, hdx@sdu.edu.cn).

Zhitong Xue is with Electric Power Research Institute of State Grid Jiangsu Electric Power Co. Ltd, Nanjing, China. (e-mail: 1347726464@qq.com).

Wah Hoon Siew is with the Department of Electronic & Electrical Engineering, University of Strathclyde, Glasgow G1 1XQ, U.K. (e-mail: wh.siew@strath.ac.uk)

deterioration of transformer insulation. Moreover, these experimental methods cannot be used to study the initial process of bubble migration in oil, namely, the process by which bubbles are generated in oil. Therefore, we must study the entire migration process and characteristics of bubbles generated in the oil itself in an oil-pressboard insulation needle-plate system.

However, these studies use uniform electric fields and ignore the generation of bubbles in the transformer oil itself. Thus, we built an experimental platform to study bubble generation and migration in the insulating oil of a needle-plate system, and the results reveal the mechanism of bubble generation under single- and multi-streamer discharge. We also analyze the migration of bubbles in oil based on the dynamic characteristics of bubbles.

This work is organized as follows: The migration and characteristics of bubbles in the insulating oil of a needle-plate system are studied from the perspective of bubble dynamics by combining experiments with numerical simulation. This work explores the variations in the size, number, and type of bubbles generated in oil-pressboard insulation exposed to an AC voltage. We also analyze how the initial position and size of bubbles affect the migration and characteristics of bubbles and discuss the possible hazards of bubbles in electric fields.

II. Experimental Platform and Method

A. Experimental setup

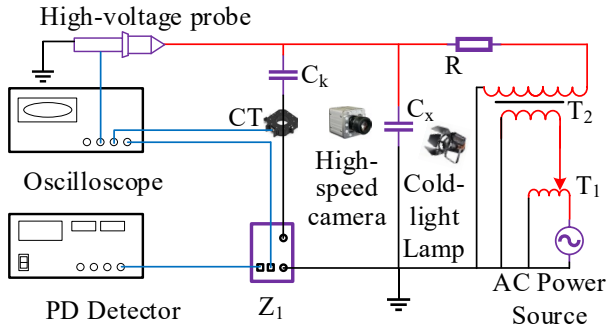

(a) Experimental circuit.

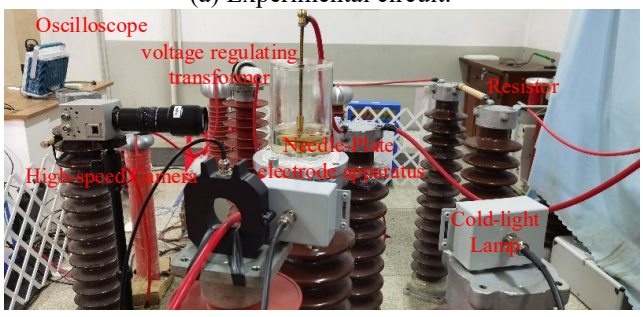

(b) Experimental devices.

Fig. 1. Experimental setup for monitoring PD and bubbles in insulating oil.

The burr defect is a common insulation defect in an oil-immersed power transformer. The electric-field distribution around a burr defect is extremely nonuniform, and bubbles are easily generated at such defects. To simulate bubble generation and bubble migration in the extremely nonuniform electric field of an oil-immersed power transformer, we built an experimental platform to monitor bubble generation and migration in the insulating oil of a needle-plate system. Figs. 1(a) and 1(b) show the experimental circuit and physical devices, respectively. In Fig.1(a), Z_1 is the detection impedance, C_k is the coupling capacitor, C_x is the oil-pressboard insulation needle-plate system, T_1 is the HV transformer, T_2 is the voltage regulating transformer, and R is the limiting resistor. The coupling capacitor is connected in parallel with the needle-plate system.

The experimental setup includes oil-pressboard insulation needle-plate system, voltage regulation, image acquisition, and PD measurement. The bubbles are observed at the needle-plate electrode in the oil tank; the latter was made of organic glass and filled with Kunlun 25# transformer oil. Figs. 2(a) and 2(b) show the needle-plate electrode model and physical diagram, respectively.

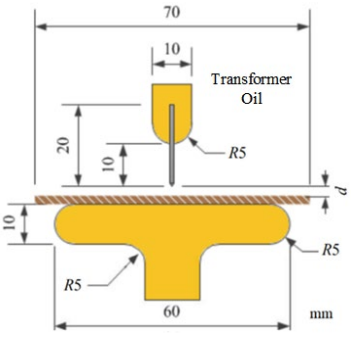

(a) Schematic diagram.

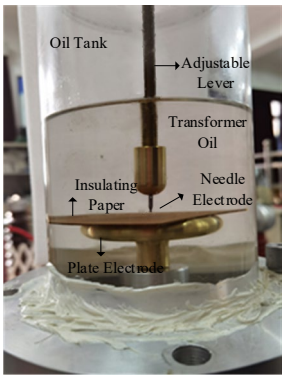

(b) physical diagram.

Fig. 2. Oil-pressboard insulation needle-plate system.

The conclusions deduced from the relation between PDIV of AC and oil gap also show a probable relation between average inception electric field strengths in oil gap and pressboard. The equivalent electric field strength is used to simulate the transformer state under the actual working conditions. When the AC voltage is 606.2kV, the maximum electric field strength borne by the transformer is about 13.9kV/mm[22]. An oil gap of 0.5mm-1.5mm is chosen to simulate the burr and tip discharge in the transformer. When the oil gap is 0.5mm-1.5mm, the pressboard with a thickness of 1mm-1.5mm can be used to simulate the electric field strength of the insulation defect in transformer [7,23]. It is easier to simulate the electric field strengths of the insulation defect in transformer by using the short oil gap and the thin pressboard. Therefore, in the oil-pressboard insulation needle-plate system in Fig. 2, the oil gap and the thickness of the pressboard were 0.5mm and 1 mm respectively. In this model, the needle electrode was made of carbon steel, and its pillar and plate electrode were made of brass. The radius of curvature of the tip of the needle electrode was 0.05 mm. The steps to adjust the oil gap are as follows.

1. Put a 0.5mm pressboard above the testing pressboard.
2. Make the upper electrode down until it meets the 0.5mm pressboard.
3. Take out the 0.5mm pressboard between testing pressboard and upper electrode.

The voltage regulation part of the experiment consisted of an AC power source, a voltage regulating transformer, a high voltage transformer, and a 50 kΩ limiting resistor. The AC power source should be connected to the voltage regulating transformer, then the voltage regulating transformer to the HV transformer, and finally the HV transformer to the limiting resistor. The AC voltage on the needle-plate electrode can be adjusted by the voltage regulating transformer.

The image acquisition part was composed essentially of a wolf-X213 high-speed camera (5000 fps), a computer and a cold-light lamp. The high-speed camera was triggered at the same time as the oscilloscope after delay correction.

The PD measurement devices of the experiment consisted of a CT, a coupling capacitor, an oscilloscope, a PD detector and its detection impedance. The PD detector is connected to the output end of the detection impedance for measuring and collecting the PRPD spectrum. According to the IEC 60270, the frequency range of the PD detector was set to 100 kHz ~500 kHz for obtaining PRPD spectrum. The oscilloscope is connected to CT and another output end of the detection impedance. The detection impedance and CT can measure the pulse waveforms at the same time. The rated capacity of coupling capacitor is 1000pF. And the bandwidth of CT is 3 MHz ~ 30 MHz. The main parameters of the PD measurement devices are shown in Table I.

TABLE I
THE MAIN PARAMETERS OF THE PD MEASUREMENT DEVICES

Device name	Parameter	Numerical value
CT	Bandwidth / MHz	3~30
Detection impedance	Impedance / Ω	50
Coupling capacitor (HZOH)	Hold-off voltage / kV	120
	Rated capacity / pF	1000
PD detector (DDX 912b)	Bandwidth / kHz	16~1500
	Sensitivity / pC	< 0.1
Oscilloscope (DPO 4104B)	Bandwidth / GHz	1
	Sensitivity / mV	1
	Sampling rate / GS/s	5

B. Experimental Method

According to IEC 60641, the transformer oil filtered by vacuum oil filter shall be treated at 65℃ and 50pA for 48 hours before the experiment. The volume fraction of gas in oil shall be less than 2%, and the micro water content shall be less than 10%μL/L. The insulating pressboard shall be dried at 110℃ and 50pA for 72 hours, and then soaked in oil at 80 ℃ and 50pA for 48 hours. The moisture content of pressboard shall be less than 1%. During the experiment, the ambient noise was kept below 5 pc. PD also occurred within the experimental circuit at places other than the needle-plate electrode. To eliminate such PDs, all experimental devices were connected via shielded wires of a length that avoided their being bent too severely, and each point of connection was wrapped with copper foil. The high-speed camera was placed about 30 cm from the oil tank, and the camera parameters were set to ensure that the images were sufficiently clear to determine the formation and migration of bubbles.

During the experiment, the constant voltage method was used to increase the voltage. For voltage boosting, the voltage was held constant for 2 minutes after every 1 kV voltage increase to ensure voltage stability. This method not only avoids having the voltage step perturb the experimental results but is also closer to the actual working conditions of the oil-immersed power transformer. For the oil-pressboard insulation needle-plate system used in this paper, through experimental statistics, we found that the partial discharge inception voltages are 26kV in 9 of the 12 experiments under the same conditions. So the partial discharge inception voltage of this experimental platform is 26kV. The radius of curvature of the needle electrode tip is 50 μm, and the standard size of the bubbles is measured by using a vernier caliper with reference to the curvature of the needle tip.

III. STUDY OF INITIAL MIGRATION CHARACTERISTICS OF BUBBLES IN OIL

A. Bubble Generation in Oil

Experimental observation shows that the number of bubbles in the transformer oil increases significantly after PD, as shown in Fig. 3.

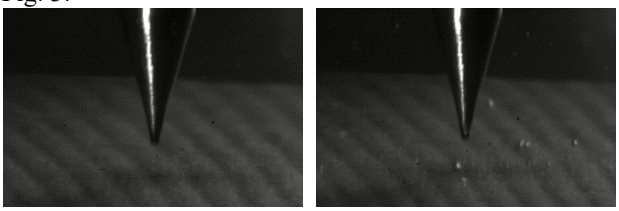

(a) Before PD. (b) After PD.

Fig. 3. Variation in bubble number before and after PD.

To explain this phenomenon, we studied the process by which bubbles are generated. In the above 12 experiments, the voltage was continue increased after raising the voltage to the partial discharge inception voltage. In one of the experiments, when the applied voltage was increased to 31.2kV, single-streamer discharges and multiple-streamer discharges occurred in the oil-pressboard insulation system, and a large number of bubbles were generated.

As shown in Fig. 4 and 5, the development process of the single-streamer discharges and multiple-streamer discharges are recorded. Among them, (a) in Fig.4 and 5 is the picture of the most intense combustion of the streamer discharge are captured, and this time is defined as zero time. After 0.2ms, the streamer discharge will be extinguished, as shown in (b) in Fig. 4 and 5. After 0.4ms, the streamer discharge is completely extinguished, as shown in (c) in Fig. 4 and 5. At this time, the development of the streamer discharge is completed, and a large number of bubbles are generated at the position of the streamer discharge channel. Comparing (a) and (b) shows that the extinguishment of the streamer channel starts at the tip of the needle electrode and then extends to the pressboard. During this time, the streamer channel gradually disconnects from the

needle electrode. At this point, the volume of the streamer discharge channel expands rapidly, and the brightness decreases significantly. The volume expansion of streamer discharge channel is completed in one frame (0.2ms). And the migration process of bubbles between oil gaps often takes about three frames (0.6ms). So the volume of streamer discharge channel expands rapidly.

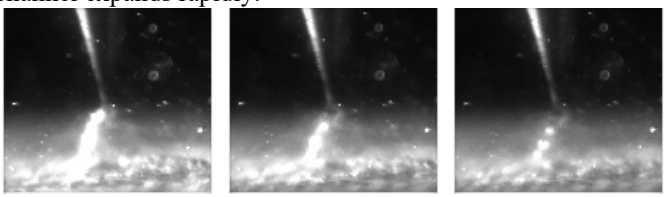

(a) 0ms. (b) 0.2ms. (c) 0.4ms.

Fig. 4. Single-streamer discharge in needle-plate system.

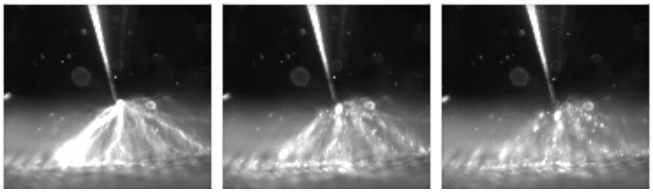

(a) 0ms. (b) 0.2ms. (c) 0.4ms.

Fig. 5. Multi-streamer discharge in needle-plate system.

Due to the randomness of streamer discharge, multiple streamer discharges are not generated at the same time. The leftmost streamer is generated slightly later than the right streamer, so the leftmost streamer is the brightest when the high-speed camera captures the Fig. 5. When the channel collides with the pressboard, its speed drops abruptly. According to the continuous surface tension model proposed by Brackbill, the liquid molecules at the gas-liquid interface are attracted by the liquid side, which will make the bubbles keep spherical. Therefore, the shape of the channel changes significantly and is transformed into spherical bubbles exposed to the surface tension of a gas-liquid interface, as shown in the Fig. 4(c) and Fig. 5(c). Because the initial movement of large bubbles is relatively slow, the relatively large bubbles formed by the impact of the channel on the pressboard will be generated at the corresponding position of the channel. At this time, the total volume of large bubbles is much larger than that of small bubbles, so the main body of the streamer discharge channel will be transformed into large bubbles. Most of the small bubbles appear around the channel. At this time, the large bubbles have not split into small bubbles, so the small bubbles are formed by the participating gas in the channel. Fig. 4(c) and 5(c) show bubbles generated by a single- (multi-) streamer channel. Large bubbles are transformed from the main body of the streamer channel, and small bubbles were formed from the residual gas of the bubbling streamer channel.

The pulse waveforms corresponding to above two partial discharges are collected by the oscilloscope connected to the CT, which are shown in Fig. 6. Fig. 4(a) shows that the single-streamer discharge has a penetrating channel without any branches in the oil gap. The channel is slender and bright. The single-streamer discharge and its pulse waveform are shown in Fig.4(a) and Fig.6(a). The fact that this channel was slender and bright meant that the PD energy is concentrated. When the single-streamer discharge arrives at the pressboard surface, a copious amount of charge is injected into the interface of oil and pressboard, where the electric field will become distorted, and an intense ionization will occur. The pulse waveform of single-streamer discharge was a unimodal without an obvious oscillatory behavior. Fig. 4(b) shows that the multi-streamer discharge channel had an oil gap penetrated by several streamers. A bright discharge at each branch point was obvious. The multi-streamer discharge and its pulse waveform are shown in Fig. 5 (a) and Fig. 6 (b). The pulse waveform of the multi-streamer discharge is a unimodal pulse with oscillations at the peak and falling edge [24].

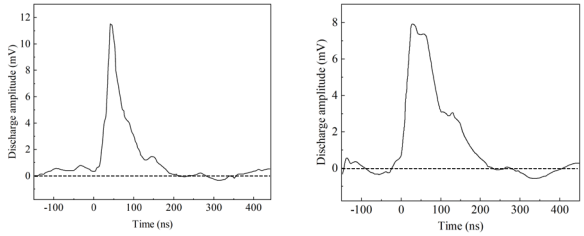

(a) Single-streamer. (b) Multi-streamer.

Fig. 6. The PD pulse waveform of Single-streamer and multi-streamer discharge

B. Number and Evolution of Bubbles in Oil

Through experimental observation, it is found that the number of bubbles increases sharply after PD occurs. Moreover, the speed at which the number of bubbles increases is related to the size of bubbles. Compared with large bubbles, the number of small bubbles increases faster. Through experimental observation, we have counted 50 processes of bubble splitting, of which the bubbles with a radius of more than 50μm split 42 times. Therefore, when the bubble radius is above 50μm, most of the bubbles will split into smaller bubbles, while when the bubble radius is below 50μm, most of them will not continue to split into smaller ones, and their state is relatively stable. The large bubbles will split to form small bubbles under the action of external force [25], so whether the bubbles will split can be used to define whether they are large or small bubbles. Combined with the experimental environment of this paper, the bubbles with a radius of more than 50 μm were defined as large bubbles, and bubbles with a radius of less than 50 μm were defined as small bubbles.

In order to more accurately study the changes in the number of bubbles generated by different PD types. We setting the time origin at the start time of streamer discharge, and ensured that the observation range of the high-speed camera is constant. Then the number of bubbles within the observation range was calculated. We recorded the changes of the number of bubbles with time after 20 single- (multiple-) streamer discharges respectively, and calculated the average value of the number of bubbles at different time nodes, as shown in Fig.7. Finally, the more precise relationship between the number of bubbles generated by single-streamer and multi-streamer discharges and

the time function was obtained.

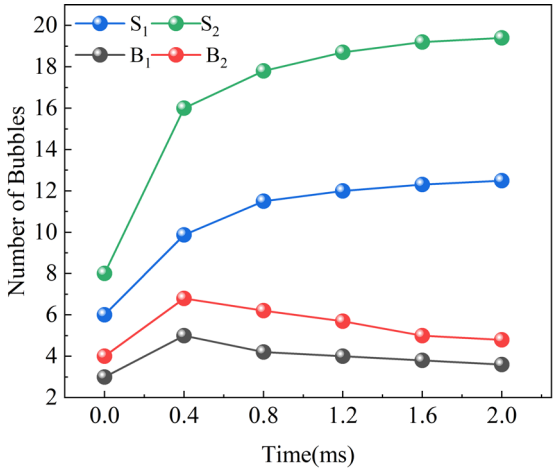

Fig. 7. Number of bubbles as a function of time caused by single- and multi-streamer discharge. S_1 and B_1 (S_2 and B_2) are small and large bubbles generated by single-streamer (multi-streamer) discharge, respectively.

Fig. 7 shows that large bubbles and small bubbles in oil increase sharply within 0.4 ms after PD. There is a close correlation between PD and bubble generation. For the same type of bubbles, significantly more bubbles are generated by multi-streamer discharge than by single-streamer discharge. For the same type of PD, significantly more small bubbles are generated than large bubbles. After 0.4 ms, the number of small bubbles increases slowly, but the number of large bubbles decreases slowly. To explain this phenomenon, the evolution of large and small bubbles in oil should be further studied.

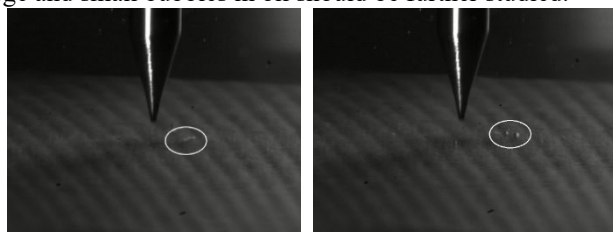

(a) The splitting process of big bubble.

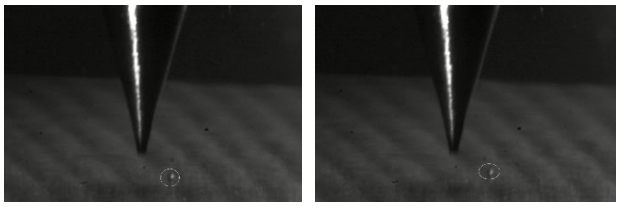

(b) Nonsplitting bubbles.

Fig. 8. Evolution of bubbles.

Experimental observation reveals that, when a streamer bubbling channel develops rapidly, large bubbles will collide with the pressboard after formation and then split into small bubbles, as shown in Fig. 8(a). This is consistent with the phenomenon shown in Fig. 7 whereby the number of large (small) bubbles decreases (increases) after 0.4 ms. In contrast with the phenomenon shown in Fig. 8(a), when the streamer bubbling channel develops slowly, large bubbles do not split after formation. Instead, large bubbles first accelerate over a short distance toward the pressboard and then gradually leave the upper surface of the pressboard due to buoyancy, as shown in Fig. 8(b).

IV. STUDY OF MIGRATION OF BUBBLES IN OIL

To further analyze the experimentally observed migration of bubbles in insulating oil, we use numerical simulation to study the migration characteristics of bubbles in the needle-plate system.

A. Numerical Model of Bubble Migration

Considering the actual working conditions inside the transformer, the geometric model was established by using COMSOL. A spherical bubble of radius r is placed in the transformer oil. A power-frequency AC electric field is applied to the transformer oil by the needle-plate electrode model. The needle electrode is the high voltage electrode, and the plate electrode is the grounded electrode. Fig. 9 shows the annotation for the geometric, which is consistent with the dimensions given in Fig.2.

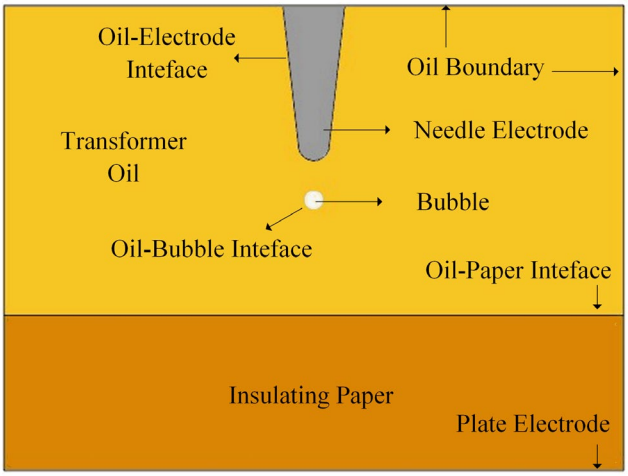

Fig. 9. Bubble simulation model for needle-plate system.

According to electromagnetic-field theory, the electric field in the model is given by

$$\boldsymbol{E} = -\nabla\varphi, \tag{1}$$

$$\boldsymbol{D} = \varepsilon\varepsilon_0\boldsymbol{E}, \tag{2}$$

$$\nabla\cdot\boldsymbol{D} = q, \tag{3}$$

where E is the electric field, φ is the electric potential, ε is the dielectric constant, ε_0 is the vacuum permittivity, D is the potential displacement, and q is the free-charge density [12,19].

In a nonuniform electric field, assuming that the fluid (i.e., transformer oil and the gas in the bubbles) is incompressible, the force on the bubbles consists mainly of electrodynamic, drag, and buoyancy forces; the latter two being due to the liquid viscosity and gravity, respectively. Therefore, the equation of motion for bubbles in the liquid is

$$m\frac{dv}{dt} = F_E + F_D + F_B + F_G, \tag{4}$$

where m is the bubble mass, v is the bubble velocity, t is time, F_E is the electric-field force of bubbles; F_D is the drag force on the bubble, F_B is the buoyancy force on the bubble, and F_G is

the force of gravity on the bubble[12,19]. The electrodynamic density $\boldsymbol{f}$ of the fluid (i.e., transformer oil plus the gas in the bubbles) exposed to the electric field is

$$\boldsymbol{f} = q\boldsymbol{E} - \frac{1}{2}E^2\nabla\varepsilon + \frac{1}{2}\nabla\left[\rho\left(\frac{d\varepsilon}{d\rho}\right)E^2\right], \quad (5)$$

where ρ is the fluid density. The term qE on the right side of the formula is the Coulomb force, which is the force on the dielectric volume element containing free charge. The second term is the dielectric electrophoresis force, which is related to the spatial variation of the electric-field strength and the dielectric constant at the corresponding spatial position. The third term is the electrostriction force. This model assumes zero free charge in the medium and ignores any deformation of the bubble. The electrodynamic force on the bubble only considers the dielectric electrophoresis force applied to the fluid (i.e., transformer oil plus the gas in the bubbles).

The total electric-field force F_E of the medium can be expressed as the volume fraction of the force density f shown in (5) to the corresponding medium and can also be calculated by the area fraction of the Maxwell stress tensor T1 of the medium on the volume surface. To simplify the calculation, we assume that the dielectric polarization is proportional to the dielectric density:

$$\varepsilon - 1 = \chi_e = \alpha\rho \ , \quad (6)$$

where ε , χ_e , and ρ are the relative dielectric constant, polarization, and medium density, respectively, and α is a constant of proportionality [12,19]. Since the polarization is related to the relative permittivity and density of the medium, and the relative permittivity and density of the insulating oil and pressboard used in the experiment do not change, the polarization does not change and cannot be controlled in the experiment. For gas and liquid with a small relative dielectric constant, (6) can generally be satisfied, so Maxwell stress tensor T_1 is

$$nT_1 = -\frac{1}{2}n\left(E\times D\right) + \left(n\times E\right)D^T, \quad (7)$$

where n is the outer normal direction from the medium interface [12,19]. The electric power of the medium is obtained by integrating (7) at the medium interface:

$$F_E = \iint_\Omega mT_1 d\Omega \ , \quad (8)$$

The drag force caused by oil viscosity can be expressed as

$$F_D = -4\pi\mu r v, \quad (9)$$

where μ is the dynamic viscosity of the transformer oil, r is the bubble radius, and v is the bubble velocity [12,19].

The resultant force of buoyancy and gravity on bubbles can be expressed as

$$F_B = \frac{4}{3}\pi r^3\left(\rho_1 - \rho_g\right)g, \quad (10)$$

where ρ_1 is the transformer oil density, ρ_g is the gas density in the bubble, and g is the acceleration due to gravity [12,19].

Table II lists the properties of related materials in the model.

TABLE II
PARAMETERS OF RELATED MATERIAL PROPERTIES

Parameter	Value
Transformer oil density (kg/m³)	895
Relative dielectric constant of oil	2.2
Dynamic viscosity of oil (Pa s)	0.01432
Gas density in bubbles (kg/m³)	1.293
Relative dielectric constant of bubbles	1
Relative dielectric constant of pressboard	4

B. Characteristics of Migration of Bubbles in Oil

To compare the simulation with the experimental phenomenon, the position of generation, the size, and the applied voltage for a typical bubble produced in the experiment are used as the parameters in the simulation. A bubble of average radius 0.05 mm is produced at the tip of the needle at 31.2 kV AC voltage. Fig. 10 shows the position of the bubble at various intervals. Taking the tip of the needle as the origin, a rectangular coordinate system is established to measure the displacement of the bubble and compare with the simulation results (see Fig. 11).

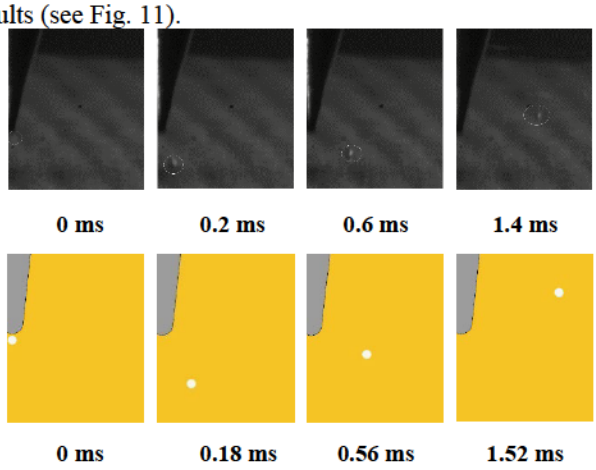

Fig. 10. Migration of bubbles at different time. Upper row shows experimental results, lower row shows simulation results.

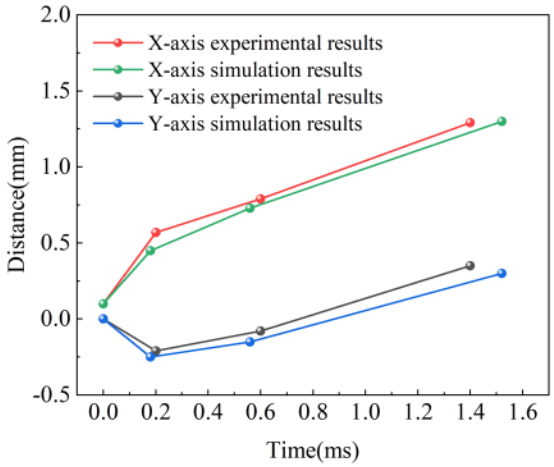

Fig. 11. *X* and *Y* coordinates of bubble as a function of time

The motion of bubbles in oil was decomposed orthogonally after the bubbles were generated. As seen in Figs. 10 and 11, the bubbles move continuously along the X axis and gradually approach the tank wall opposite the needle point. Along the Y

axis, the bubbles first move in the negative direction and then gradually reverse direction after about 0.2 ms and move in the positive Y direction. Starting from the needle tip, the bubbles first approach the pressboard and then gradually rise to the oil level.

The comparison between the migration of bubbles in Fig. 10 and the displacement of bubbles along the X and Y axes in Fig.11 shows that the simulated bubble movement is essentially consistent with the experimental result, which strongly supports the rationality of the bubble-migration model in a needle-plate system. Because the bubble is too small in the experiment, the error in bubble displacement and bubble speed is large, but the simulation software can automatically extract its index. Therefore, the simulation can be used to analyze the bubble initial position and size and the physical and chemical parameters of the insulation and their effect on bubble migration.

The dynamic behavior of bubbles in insulating oil under electric field mainly includes the migration trajectory (distance) of bubbles and velocity change of bubbles. By studying the movement trajectory and velocity of the bubbles, the magnitude and direction of the force on the bubbles at different times and positions can be obtained.

1) Influence of initial bubble position

Experimental observation shows that most of the bubbles in the oil form at the tip of the needle and at the strongest electric field. Therefore, the simulated bubbles are generated near the tip. The bubble surface and the needle surface are separated by 0.05 mm. The initial position of the bubbles is defined by the initial angle of the bubbles. The initial angle α of the bubble is the angle between the line from the bubble center to the ball center at the end of the needle electrode and the *Y* axis. Bubbles with radius r = 0.05 mm and initial positions α = 0°, 15°, 30°, 45°, 60°, and 75° were simulated.

To facilitate the analysis, the calculated migration displacement and migration velocity are orthogonally decomposed. The migration displacement and speed of bubbles along the *X* and *Y* axes at different initial positions are shown in Figs. 12 and 13.

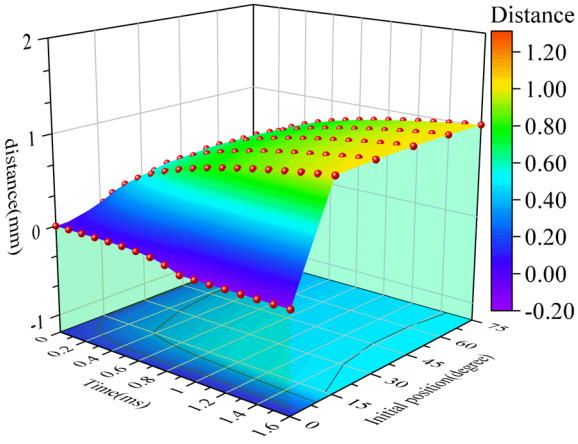

(a) *X* axis.

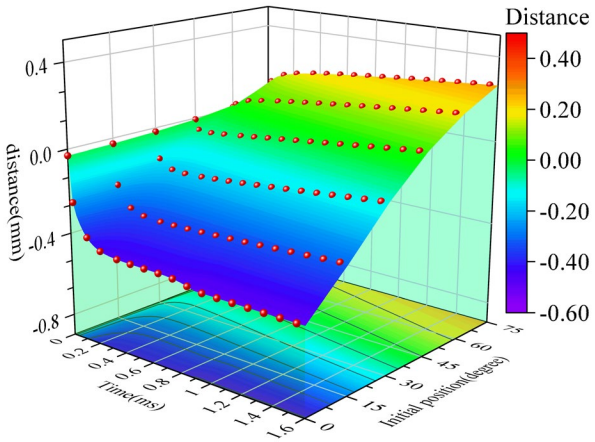

(b) *Y* axis.

Fig. 12. Displacement of bubbles along *X* and *Y* axes for different initial bubble positions.

As shown in Fig. 12(a), the bubble continues to move in the positive *X* direction, and the bubble starts from the tip of the needle and gradually approaches the oil tank wall. As shown in Fig. 12(b), the bubble first drops rapidly in the negative *Y* direction when the initial position α ≤ 45°. Later, the bubble rises slowly in the positive *Y* direction. The bubble starts from the tip of the needle, approaches the pressboard, and then gradually rises to the oil level. The bubble rises directly in the positive *Y* direction when α > 45°. At this time, the bubble gradually moves from the tip of the needle to the oil surface.

As shown in Fig. 12(a), when α ≤ 45°, with increasing initial bubble angle (i.e., a higher initial bubble position), the displacement of the bubble in the *X* direction increases at the same time. When α > 45°, at the same time, the displacement of bubbles in the *X* direction decreases. As shown in Fig. 12(b), when α ≤ 45°, with the rise of the initial position of the bubble, the displacement of the bubble moving in the negative *Y* direction gradually decreases and the displacement in the positive *Y* direction gradually increases. When α > 45°, the bubble no longer moves in the negative *Y* direction, but the displacement of the bubble in the positive *Y* direction grows increasingly large.

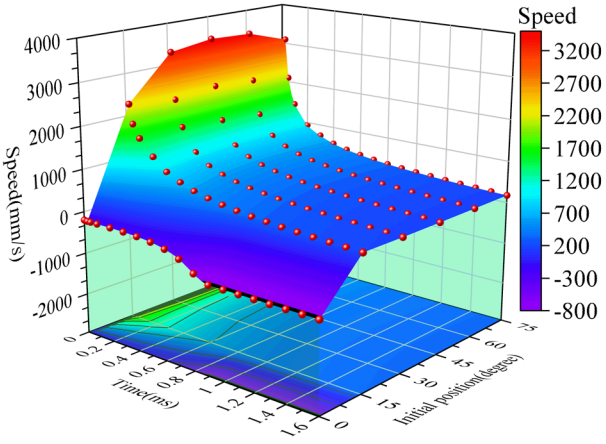

(a) *X* axis.

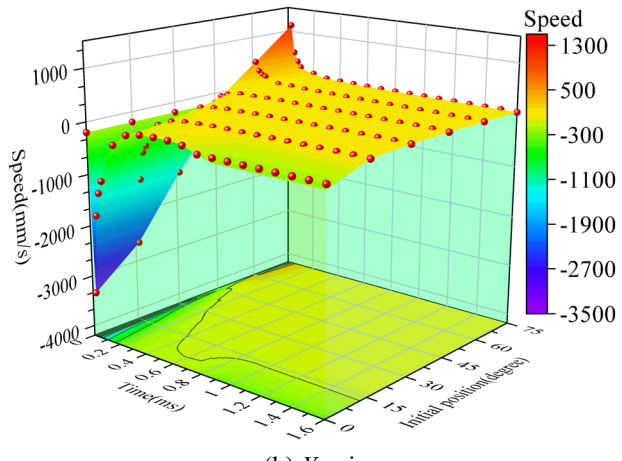

(b) *Y* axis.

Fig. 13. Speed of bubbles along *X* and *Y* axes for different initial bubble positions.

Fig. 13(a) shows that the bubble speed of a newly generated bubble in the *X* direction is very large but gradually decays to a small constant value. Fig. 13(b) shows that, when $\alpha \leq 45°$, the speed of a newly generated bubble increases rapidly in the negative *Y* direction and, after a short time, its speed increases rapidly in the positive *Y* direction. After a relatively short time, the speed in the positive *Y* direction slowly approaches a small constant value. When $\alpha > 45°$, the bubble speed increases rapidly in the positive *Y* direction and then gradually decreases to a small constant value.

Fig. 13(a) shows that, when $\alpha \leq 45°$, the higher initial position of the bubble correlates with an increase in the speed of the engraved bubble in the *X* direction. When $\alpha > 45°$, the speed of the engraved bubble in the *X* direction decreases. Fig. 13(b) shows that, when $\alpha \leq 45°$, the higher initial position of the bubble correlates with a decrease in the speed of the engraved bubble in the negative *Y* direction. When $\alpha > 45°$, the speed of the engraved bubble in the positive *Y* direction increases.

2) Influence of bubble size

Given the uneven bubble size in the oil caused by PD, we use bubble radius r = 0.02, 0.04, 0.06, and 0.08 mm to align with the size of bubbles generated experimentally. The migration of bubbles in oil is calculated and studied for an initial bubble position $\alpha = 30°$. Figs. 14 and 15 show the migration distance and speed of bubbles in the *X* and *Y* directions as functions of time and for different sizes.

Fig. 14(a) shows that, upon increasing the bubble radius, the bubble migrates farther in the *X* direction in the same time interval. In other words, bubbles with larger radii migrate farther from the tip of the needle. Fig. 14(b) shows that, upon increasing the bubble radius, the bubble displacement in the negative *Y* direction first increases and then decreases, and the displacement in the positive Y direction grows increasingly large.

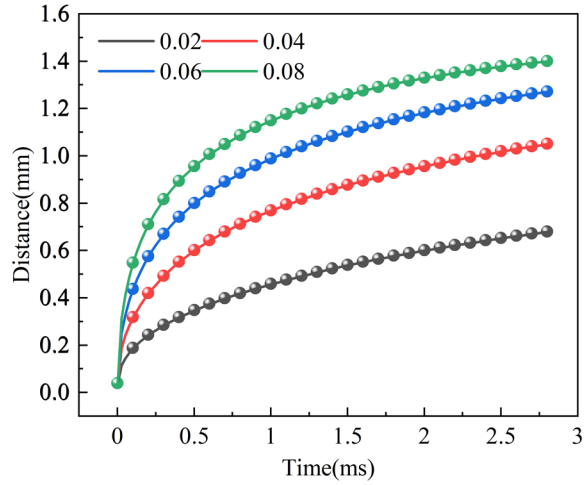

(a) X-axis

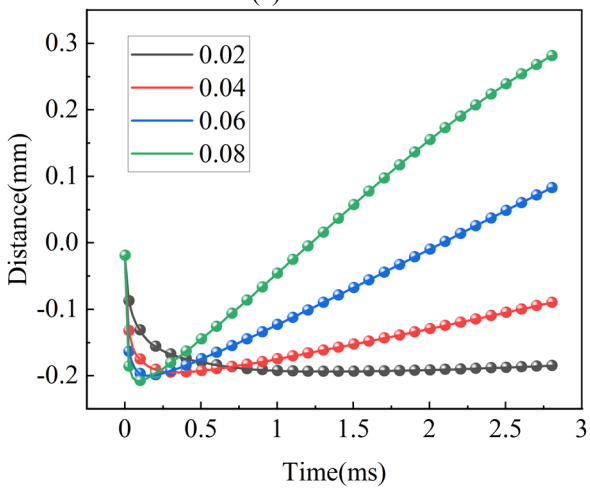

(b) Y-axis

Fig. 14. Migration distance of bubbles in X and Y directions as functions of time and for different initial bubble sizes.

To better monitor the bubble speed, the simulation is stopped at 600 μs. When the time t≤50μs, that is, when the speed of the bubble along the negative Y direction is large, if the radius of the bubble r≤0.06mm, the speed increases with the increase of the radius of the bubble, but if r=0.08mm, the speed of the bubble is the smallest. Combined with migration distance of bubbles on Y directions in Fig. 14(b), with the increase of time, the position of the bubble will appear in the positive Y direction. It can been seen that as the bubble radius increases, the speed in the positive Y direction increases. So, Fig. 16(b) shows that, as the bubble radius increases, the speed of the engraved bubble in the negative Y direction first increases and then decreases, but the speed in the positive Y direction increases.

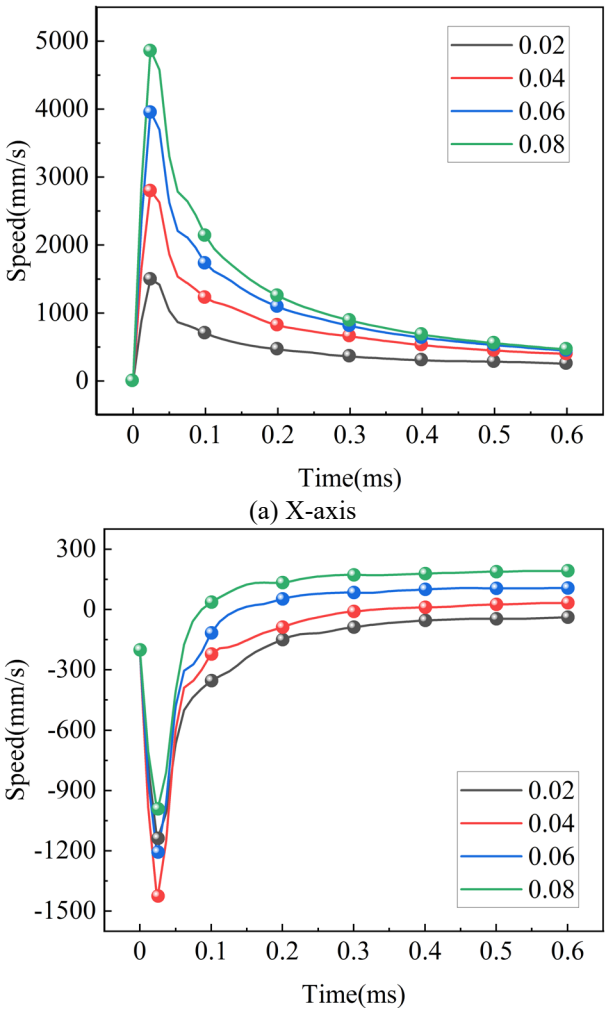

Fig. 15. Speed of bubbles in X and Y directions as functions of time and for different initial bubble sizes.

V. DISCUSSION

The forces exerted on bubbles in insulating oil include gravity, buoyancy, and drag force. However, the largest force is the Coulomb force due to the electric field, and this force has the greatest influence on the migration of the bubbles. The forces exerted on bubbles are decomposed into orthogonal components, and the free-body force diagram is shown in Fig.16. Figs. 16(a)–16(c) show the forces exerted on the bubbles moving in the X direction, in the negative Y direction, and in the positive Y direction, respectively.

The force F_G of gravity exerted on the bubble provides a constant force in the negative Y direction. The buoyancy force F_B exerted on the bubble provides a constant force in the positive Y direction. The magnitude and direction of the drag force F_D exerted on the bubble are determined by its velocity V. The higher the velocity, the greater is the magnitude of the drag force exerted on the bubble, and the direction of the drag force is always opposite to the direction of the bubble velocity. The magnitude and direction of the electric-field force F_E exerted on the bubble depend on the electric field distribution around the bubble. The greater the electric field, the larger is the electric-field force exerted on the bubble, and its direction points from the region with high field strength E_B to the region with low field strength E_S.

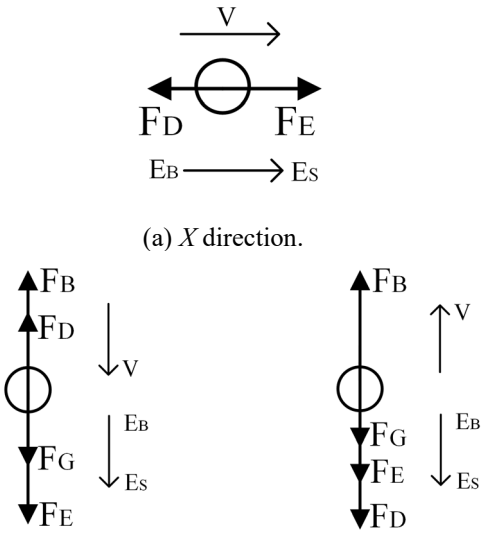

Fig. 16. Free-body diagram of forces exerted on bubble in oil.

Taking as an example the initial bubble position as $\alpha = 30°$ and the bubble radius as $r = 0.06$ mm, we now discuss the bubble migration characteristics and analyze them from a mechanics perspective. Figs. 17(a) and 17(b) show the migration distance and speed of bubbles in the X and Y directions, respectively.

The bubbles are generated in the oil near the tip of the needle, where the electric field is strongest. The electric-field force exerted on the bubbles is much greater than the buoyancy and drag forces. Thus, the bubble motion is mainly due to the electric-field force. Because the electric-field force points from regions of high field strength to regions of low field strength, the bubbles migrate toward regions of weak field strength, which are far from the tip of the needle.

Fig. 17(a) shows that, in the X direction, the net force exerted on the bubble is the electric field force plus the drag force [cf. Fig. 16(a)]. The initial electric-field force causes a sharp initial acceleration of the bubble. However, with increasing bubble velocity and the change in bubble position, the drag force gradually increases, and the electric-field force gradually decreases. When the drag force balances the electric-field force, the bubble velocity begins to decay gradually. As the bubble gradually distances itself from the region of strong field, the bubble velocity in the X direction gradually approaches zero. In this way, the bubble moves from a region of strong field to a region of weak field due to the electric field force and the drag force. The end result is that the bubble gradually departs from the needle tip and approaches the wall of the oil tank.

For Fig. 17(b), the bubble is subjected to the electric field, drag, gravity, and buoyancy (in the Y direction). Fig. 16(b) shows the corresponding free-body diagram. At the onset of the time-period I, the bubble is close to the needle tip, which is a region of strong electric field. At this moment, the electric-field force and gravity are greater than drag and buoyancy. The

bubble velocity in the negative *Y* direction increases sharply, which means that the bubble accelerates downward. The bubble thus drops rapidly away from the needle tip toward the pressboard. This stage is called the rapid decline stage of the bubble motion.

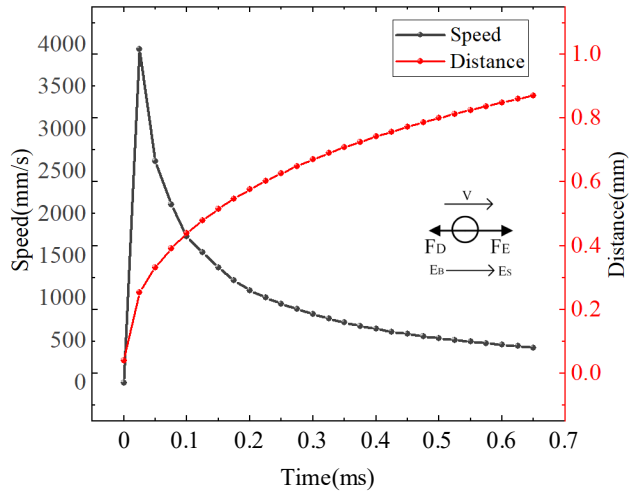

(a) *X* direction.

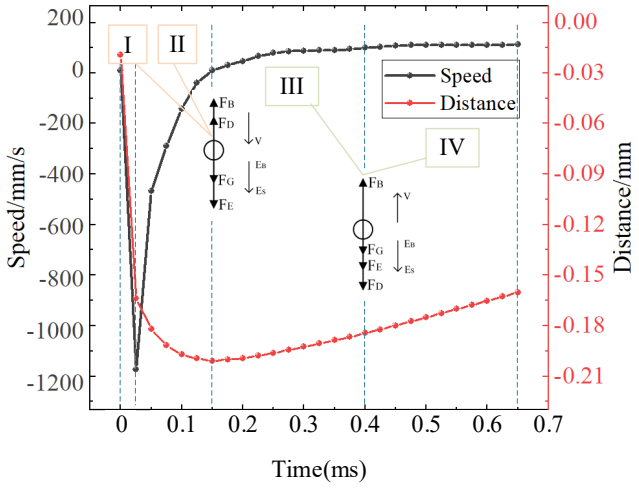

(b) *Y* direction.

Fig. 17. Migration distance and speed as functions of time for bubbles moving in (a) *X* direction and (b) *Y* direction

At the onset of time-period II, the electric field around the bubble is weak, and the bubble velocity along the negative *Y* direction is maximal. The sum of drag and buoyancy exerted on the bubble is greater than the sum of gravity and the electric-field force. The bubble velocity in the negative *Y* direction decreases gradually. The bubble accelerates upward and moves downward toward the pressboard with gradually decreasing velocity. This is called the "slow descent" stage of the bubble motion.

At the beginning of time-period III, the bubble is closest to the pressboard, its speed drops to zero, and the electric field, drag, gravity, and buoyancy all balance. Fig. 16(c) shows the free-body diagram for the bubble. The drag force of the bubble is reversed, and the buoyancy force exerted on the bubble is greater than the drag force, the electric-field force, and gravity combined, and the bubble speed increases rapidly in the positive *Y* direction. At this moment, the speed of the bubble is gradually increasing. This is called the "rapid rising" stage of the bubble motion.

At the onset of time-period IV, the bubble velocity is increasing, so the drag force also increases. The buoyancy force exerted on the bubble cancels the combined forces of drag, electric field, and gravity because the bubble is in a region of weak electric field, so the electric-field force on the bubble is small. The bubble speed in the *Y* direction slowly approaches a constant speed under the dominant forces of buoyancy, gravity, and drag. At this moment, the bubble moves uniformly upward toward the oil free surface. This is called the "uniform upward" stage of the bubble motion.

Comparing Fig. 12(b) with Fig. 13(b) shows that, for an initial position $\alpha \leq 45°$, with increasing initial position of the bubble, the displacement of the bubble in the negative *Y* direction gradually decreases, and the rapid decline and slow decline stages of the bubble become increasingly relaxed, so the bubble more easily enters the rapid rise stage. This is because, with the increasing initial position of the bubble, the electric-field intensity around the bubble decreases, and the electric-field force exerted on the bubble plays a leading role. The rapid decline and slow decline stages of the bubble disappear when $\alpha > 45°$. After a bubble is generated, it directly enters the rapid rise stage. With the increasing initial bubble position, a more intense rapid rise stage means that it takes longer for the bubble to enter the uniform rise stage because, at this time, the buoyancy provides a constant force that dominates the bubble kinematics, whereas the electric-field force gradually decreases. Comparing Fig. 14(b) with Fig. 15(b) shows that, when $r \leq 0.04$ mm, an increase in the bubble radius causes the bubble to move farther and faster in the negative *Y* direction; that is, the rapid descent stage becomes increasingly intense because the electric-field force dominates the bubble kinematics due to the increased bubble radius. The electric-field force exerted on the bubble in the negative *Y* direction also increases, so the bubble is not only significantly displaced in the negative *Y* direction but also moves at high speed in the rapid falling stage. When $r > 0.04$ mm, upon increasing the bubble radius, the buoyancy of the bubble becomes increasingly important, and the dominant role of the electric-field force on the bubble kinematics becomes increasingly small, so the bubble speed in the negative *Y* direction also becomes increasingly small. As the bubble migration enters the rapid rising stage, the buoyancy of the bubble plays an increasingly significant role, and the electric-field force plays an increasingly insignificant role. Therefore, upon increasing the bubble radius, the motion of the bubble in the positive *Y* direction increases, the speed of the bubble in the positive *Y* direction increases, and the rapid rising and uniform rising stages of the bubble become increasingly intense.

VI. Conclusion

The generation and migration characteristics of bubbles in insulating oil and exposed to an AC electric field in a needle-plate system are studied systematically by experiment and

numerical simulation. The results of the simulation are consistent with the experimental data and the main conclusions were obtained as follow:

(1) The streamer discharge channel formed by PD develops into a streamer bubbling channel. After the streamer bubble channel collides with the pressboard surface, its shape transforms into spherical bubbles due to the surface tension at the gas-liquid interface. Large, unstable bubbles are transformed from the main body of the bubbling streamer channel. The small, stable bubbles form due to the transformation of residual gas in the bubbling fluidization channel and by the splitting of large, unstable bubbles.

(2) From the perspective of bubble dynamics, the migration of bubbles may be divided into four stages to study the migration of bubbles. After a bubble is generated in the oil, it moves continuously in the *X* direction; it starts at the tip of the needle and gradually approaches the wall of the oil tank. The bubble first moves in the negative *Y* direction, then gradually accelerates until its motion is in the positive *Y* direction. The bubble starts at the tip of the needle, then approaches the pressboard, and then gradually rises to the free surface of the oil.

(3) Upon increasing the initial angle of the bubble, the migration displacement of the bubble in the *X* direction first increases and then decreases. The displacement of the bubble in the negative *Y* direction decreases, whereas it increases in the positive *Y* direction. At the same time, Newton's second law applied to the bubble moving in the *X* and *Y* directions is consistent with variation in displacement. Upon increasing the bubble radius, the displacement of the bubble in the *X* direction increases, the displacement of the bubble in the negative *Y* direction first increases and then decreases, and the displacement in the *Y* direction increases. Newton's second law applied to the bubble moving in the *X* and *Y* directions is consistent with the change in bubble displacement.

(4) Although the regions of strong electric field push the bubbles toward regions of weak electric field, bubbles may still be forced into regions of strong electric field due to forced oil circulation, temperature differences, thermal convection, and other factors, which should be considered when designing and operating such equipment. In particular, the insulation structure should be optimized to make the electric field inside the equipment as uniform as possible, and the circulation mode of insulating oil should be optimized to avoid pushing bubbles into regions of strong electric field.

ACKNOWLEDGMENT

This work was supported by the State Key Laboratory of Alternate Electrical Power System with Renewable Energy Sources (NCEPU, LAPS22001).

REFERENCES

[1] H. Cui, L. Yang, Y. Zhu, S. Li, A. Abu-Siada and S. Islam, "A comprehensive analyses of aging characteristics of oil-paper insulation system in HVDC converter transformers," IEEE Trans. Dielectr. Electr. Insul., vol. 27, no. 5, pp. 1707–1714, Oct. 2020.

[2] S. Li, Z. Liu and S. Ji, "Characteristics of Creeping Discharge Caused by a Needle Electrode in Oil-Pressboard Insulation under +DC Voltage," IEEE Trans. Dielectr. Electr. Insul., vol. 28, no. 1, pp. 215–222, Feb. 2021.

[3] X. Wang, Q. Li, C. Li, R. Yang and Q. Su, "Reliability assessment of the fault diagnosis methodologies for transformers and a new diagnostic scheme based on fault info integration," IEEE Trans. Dielectr. Electr. Insul., vol. 20, no. 6, pp. 2292–2298, Dec. 2013.

[4] Y. Zhou, F. Jin, M. Huang, Y. Sha, L. Zhang and J. Huang, "Influence of temperature on developing process of surface flashover in oil-paper insulation under combined AC-DC voltage conversion," IEEE Int. Conf. Electr. Insul. Dielect. Phenom. (CEIDP), vol. 1, pp. 486–489, October 2013.

[5] S. Li, J. Yang, S. Li, Y. Zhu, H. Cui, W. Yan, Z. Ge and A. Abu-Siada, "Effect of AC-voltage harmonics on oil impregnated paper in transformer bushings," IEEE Trans. Dielectr. Electr. Insul., vol. 27, no. 1, pp. 26–32, Feb. 2020.

[6] M. Yea, K. J. Han, J. Park, S. Lee and J. Choi, "Design optimization for the insulation of HVDC converter transformers under composite electric stresses," IEEE Trans. Dielectr. Electr. Insul., vol. 25, no. 1, pp. 253–262, Feb. 2018.

[7] B. Qi, X. Zhao, C. Li and H. Wu, "Electric field distribution in oil-pressboard insulation under AC-DC combined voltages," IEEE Trans. Dielectr. Electr. Insul., vol. 23, no. 4, pp. 1935–1941, Aug. 2016.

[8] S. Li, W. Si and Q. Li, "Partition and recognition of PD development stages in oil-pressboard insulation with needle-plate electrodes under combined AC-DC voltage stress," IEEE Trans. Dielectr. Electr. Insul., vol. 24, no. 3, pp. 1781–1793, Jun. 2017.

[9] Y. Li, Q. Zhang, J. Li, T. Wang, W. Dong and H. Ni, "Study on micro bridge impurities in oil-paper insulation at DC voltage: their generation, growth and interaction with PD," IEEE Trans. Dielectr. Electr. Insul., vol. 23, no. 4, pp. 2213–2222, Aug. 2016.

[10] X. Li, J. Tang, S. Ma and Q. Yao, "The impact of temperature on the partial discharge characteristics of moving charged metal particles in transformer oil," Proceedings of the IEEE International Conference on High Voltage Engineering and Applications, pp. 1–4, 2016.

[11] M. Tsuchie, M. Kozako, M. Hikita and E. Sasaki, "Modeling of early stage partial discharge and overheating degradation of paper-oil insulation," IEEE Trans. Dielectr. Electr. Insul., vol. 21, pp. 1342–1349, Jun. 2014.

[12] LIU Qiushi, LI Qingmin, Niyomugabo E.Ladislas, LI Yunpeng, WU Xingwang, WU Jie, "Dynamic characteristics and migration mechanism of bubbles in insulating oil under extremely uneven electric field," Proc. CSEE, (in Chinese).

[13] M. Gao, Q. Zhang, Y. Ding, T. Wang, H. Ni and W. Yuan, "Investigation on bubbling phenomenon in oil-paper insulation," IEEE Trans. Dielectr. Electr. Insul., vol. 24, no. 4, pp. 2362–2370, Sep. 2017.

[14] S. Mo, Z. Zhao, X. Li, X. Cui, J. Xu and J. Zhang, "PD characteristics of bubble flow under AC non-uniform electric field in FC-72," IEEE Trans. Dielectr. Electr. Insul., vol. 27, no. 4, pp. 1119–1127, Aug. 2020.

[15] Y. Liu, N. Chao, T. Zhao, Y. Tong and C. Jia, "Mechanism and numerical model of bubble effect in oil-paper insulation based on microtubule model," IEEE Trans. Dielectr. Electr. Insul., vol. 27, no. 5, pp. 1529–1537, Oct. 2020.

[16] CHEN Feng, Peng Yao, Song Yaozu, *et al*, "Visualization of single bubble behavior under electric field[, "J. Tsinghua Univ., pp. 722–725, May, 2007 (in Chinese).

[17] Y. Zhang, X. Tao, C. Pan and J. Tang, "Role of air bubbles in the breakdown of flowing transformer oil," IEEE Trans. Dielectr. Electr. Insul., vol. 27, no. 5, pp. 1752–1760, Oct. 2020.

[18] Y. Zhang, J. Tang, C. Pan and X. Luo, "Comparison of PD and breakdown characteristics induced by metal particles and bubbles in flowing transformer oil," IEEE Access, vol. 7, pp. 48098–48108, Apr. 2019.

[19] T. Zhao *et al*, "Cellulose particle dynamics simulation in transformer oil under non-uniform electric field," *2017 IEEE 19th International Conference on Dielectric Liquids (ICDL)*, pp. 1–4, 2017.

[20] J. Tang, Y. Zhang, C. Pan, R. Zhuo, D. Wang and X. Li, "Impact of oil velocity on PD characteristics induced by bubbles in transformer oil," in IEEE Trans. Dielectr. Electr. Insul., vol. 25, no. 5, pp. 1605–1613, Oct. 2018.

[21] J. Tang, S. Ma, M. Zhang, Z. Liu, X. Li and Y. Gui, "Influence of microbubbles motion state on PD in transformer oil," IEEE Trans. Dielectr. Electr. Insul., vol. 22, no. 5, pp. 2646–2652, Oct. 2015.

[22] Y. Wei, H. Mu, J. Deng, G. Zhang, "Effect of space charge on breakdown characteristics of aged oil-paper insulation under DC voltage," IEEE Trans. Dielectr. Electr. Insul., vol. 23, no. 5, pp. 3143-3150, October 2016.

[23] Y. Sha, Y. Zhou, J. Li and J. Wang, "Partial discharge characteristics in oil-paper insulation under combined AC-DC voltage," IEEE Trans. Dielectr. Electr. Insul., vol. 21, no. 4, pp. 1529-1539, August 2014.

[24] Li S., Li Q. and He D. "PD classification in oil-pressboard insulation by simulating a needle-plate model with +DC voltage," IEEE Trans. IEEE Trans.

Dielectr. Electr. Insul., vol.26, no.1, pp. 261-269, January 2019.
[25] S. M. Korobeynikov, A. V. Ridel, D. A. Medvedev, D. I. Karpov, A. G. Ovsyannikov and M. B. Meredova, "Registration and simulation of partial discharges in free bubbles at AC voltage," IEEE Trans. Dielectr. Electr. Insul.,vol. 26, no. 4, pp. 1035-1042, Aug. 2019.

HONGBIN WU was born in Taian, Shandong, China. He received the B.Sc. degree from Shandong University of Technology, Shandong, China, in 2019. He is currently pursuing the Master's degree in Shandong University.

His current research interest focuses on the aging characteristics of oil-pressboard insulation in transformer.

HONGSHUN LIU was born in Qingdao, Shandong, China. He received the B.Sc. and Ph.D. degrees in electrical engineering from Shandong University, Shandong, China, in 2004 and 2010, respectively.

Currently, he is an Associate Professor of Electrical Engineering with Shandong University. His research interests include the modeling and simulation for power system electromagnetic transient processes, overvoltage and insulation coordination, partial discharge theory and its application, etc.